Nanoscopic Multimode Fracture Mechanisms in Anisotropic Silicon

Victor V. Kozhushko and Peter Hess[a]

Institute of Physical Chemistry, University of Heidelberg, 69120 Heidelberg, Germany

[a] Peter.Hess@urz.uni-heidelberg.de

Keywords: strength of silicon, nonlinear surface acoustic waves, mixed fracture mode.

Abstract. In spite of the increasing role played by mechanical stresses in applications of various silicon devices, such as MEMS, NEMS, and sensors, our understanding of the microscopic features of failure is still in its infancy. Therefore, better insight into the molecular fracture processes is an important issue. Currently ab initio theory provides the ideal tensile and shear strength of the {111} cleavage plane in single-crystal silicon and diamond only for selected geometries. These values can be compared with the real strength of nano-, micro-, and single-crystalline devices. A novel contact-free and notch-free optical laser method is introduced to measure the fracture strength with plane nonlinear surface acoustic waves (SAWs), developing shock fronts during propagation. SAW pulses provide a unique way to discriminate between tensile and shear stresses for well-defined crystallographic planes and directions ('geometries') in anisotropic materials. Calibration yields the critical real fracture stress or intrinsic strength. Uniaxial pure mode I, biaxial mode I+II, and also complex multimode I+II+III behavior was observed for selected geometries in silicon. New insight was obtained on the microscopic failure mechanisms connected with anisotropic fracture.

Introduction

Silicon is the basic semiconductor material in microelectronics, and its mechanical strength is of practical interest owing to increasing wafer sizes. Fracture strength is also a critical issue in the expanding technology of silicon-based devices such as microelectromechanical systems (MEMS) and sensors, with respect to their reliability. Here the problem of materials strength of devices with steadily decreasing size arises. An advanced material with exceptional mechanical properties is chemical vapor deposited (CVD) diamond. In the form of nano- and microcrystalline films and plates, CVD diamond is expected to play an increasing role as hard coating, high temperature semiconductor, resistant and highly transparent window, etc. The strength of single-crystal diamond is in the same range as the critical stress of CVD diamond, a surprising finding presently not well understood.

Recently several theoretical papers have been published that have determined the ideal strength or elastic limit of silicon and diamond by *ab initio* calculations [1,2]. The ideal theoretical strength characterizes perfect crystals, while real materials contain impurities, dislocations, vacancies, and other types of intrinsic defects, including extensive grain boundaries in nanocrystalline films, which may influence the effective strength substantially. It is important to realize that theory provides fracture strengths for well-defined crystallographic planes and directions ('geometries') of anisotropic crystals. These strength values are the basis of a realistic judgement of the mechanical quality not only of real single crystals but also of nano- and microcrystalline films and plates used in many practical applications.

One of the serious disadvantages of the established constant force fracture technique is the requirement of artificial precracks or notches [3−6]. In these experiments external (quasi-static) loads are used to reach the critical strain at the tip of the seed crack. This requires mechanical contact and a suitable geometry of the specimen in order to realize a uniform tensile stress field. An artificial notch provides a weak location in the specimen and under mechanical load this is usually the starting point of crack extension and propagation. At the sharp tip of a microcrack the measured

strength may be orders of magnitude lower than the intrinsic strength of the ideal material as a result of stress concentration. Because of the unknown microstructure of a notch tip, not crack nucleation and strength but crack propagation has been studied with this method.

The fracture strength of silicon and diamond has mainly been studied, for example, by indentation methods, bursting disk tests, or loading with a bearing ball [7−13]. Experiments can be performed for particular crystal cuts but the anisotropy of fracture behavior may be largely obscured, for example, by lateral cracking taking place during indentation. Thus a direct comparison between theory and experiment for well-defined fracture geometries seems to be difficult for these loading techniques. Laser-based nonlinear surface acoustic wave (SAW) pulses provide a new versatile tool to initiate intrinsic fracture in a geometrically controlled manner and to extract information on the anisotropic features of fracture.

Since SAWs are confined to a plane, these guided waves have lower diffraction losses than elastic bulk waves [14]. In the absence of dispersion, strongly nonlinear elastic surface waves with steep shock fronts develop during propagation. The nonlinear response manifests in harmonics generation and frequency-up conversion processes, causing an enrichment of higher frequency components in the SAW pulse spectrum. The strong nonlinearity can produce enormous strains on short time scales or stresses that exceed the critical fracture strength of brittle materials. In SAWs the maximum tension or compression in the stress field is always localized at the surface. Therefore, initiation of crack nucleation and propagation start at the surface. With the optical SAW method the strength of materials can be studied under transient dynamic load without any mechanical contact with the specimen. In previous investigations it has been shown that the critical value of the stress−strain field can be reached in nonlinear SAW pulses after a propagation distance of less than a millimeter in silicon [15,16]. For plane SAW pulses with their elliptical polarization the displacements connected with specific crystallographic planes and propagation directions along these planes are well defined.

Experimental

The excitation of SAW pulses was accomplished by absorbing focused laser radiation in a thin layer of ink, containing highly absorbing carbon particles, localized on the surface at the excitation region and covered by a strip of transparent film. A cylindrical lens was used to focus the laser radiation strongly into a line of ~8 mm length and ~15 µm width to excite SAW pulses with plane wave fronts, as illustrated schematically in Fig. 1. The fast overheating and explosive evaporation of the absorption layer produces a recoil momentum that acts normal to the surface, introducing strong particle displacements. The transient shape of the optically launched finite SAW pulses depends on the mechanical properties of the medium, the energy and duration of the exciting laser pulse, and the irradiated spot size. In the present experiments a Nd:YAG laser with 1.064 µm radiation, a pulse duration of ~8 ns, and a pulse energy of 30−160 mJ was employed.

This technique allows the excitation of nanosecond SAW pulses that develop strains of ~0.01 near the surface. The upper frequency limit of the excited wideband SAW pulses mainly depends on the width of the focused line source, thermophysical properties, and the laser pulse duration. The highest frequencies in the SAW pulse spectrum were estimated to be ~200 MHz. SAWs with finite amplitude induce a strong nonlinear response in an elastic medium, including harmonics generation with frequency-up and frequency-down conversion processes. Therefore, the frequency spectrum of a launched nonlinear SAW pulse will broaden considerably during propagation. As the penetration depth of SAWs is roughly one wavelength, formation of higher harmonics results in a concentration of energy nearer to the surface, exerting stronger disturbances to the chemical bonds in the surface region.

The probe-beam-deflection (PBD) technique was employed for SAW pulse detection. A diode-pumped cw Nd:YAG laser with 532 nm wavelength and ~100 mW power was used to monitor the

transient slope at the surface [14]. The laser beam was divided into two equal parts and each beam was sharply focused on the surface, providing two separate probe spots along the direction of SAW propagation (see Fig. 1). The measured signal of the photodiode current was sensitive to the deflection of the probe beam caused by transient surface deformations. The spot size of the probe beams at the surface was ~4 μm. The frequency bandwidth of the setup covered the range of 5−500 MHz. Usually the two probe beam spots of the pump−probe setup had a distance of less than 1 mm and ~17 mm from the excited line source. If the SAW solution is known, the relation between the normal component of the surface displacement and the measured surface slope is given by $\partial u_3/\partial t = -C_R\,\partial u_3/\partial x_1$, where u_3 is the displacement normal to the surface, x_1 the propagation direction, and C_R the phase or Rayleigh velocity of the SAW pulse. The calculated values of the normal component of the particle displacement vector provide the stress and strain field within the material.

The float−zone silicon samples with carefully polished mirror−like surfaces and a size of $40{\times}40{\times}3$ mm^3 were purchased from CrysTec. The miscut of the planes was less than 0.3° (typically less than 0.15°) and the surface resistance was >1000 Ωcm. The surface flatness of the silicon samples was checked by atomic force microscopy (AFM) giving a root mean squared (rms) roughness <0.2 nm for an area of $1{\times}1$ μm^2.

The nonlinear evolution equation was employed for calibration of the experimental setup [14,17]. The calibration procedure exploits the predictor-corrector method for an iterative solution of the nonlinear evolution equation. The aim was to determine the multiplier with the dimension [1/volt] for the transient SAW profile measured at the first probe spot. The solution with correct calibration factor should reconstruct the transient profile measured at the second probe spot and allow the determination of the absolute surface strain at any other location, such as the fracture positions.

Results

Since single-crystal diamond samples are not readily available in the size of about $15{\times}10{\times}0.2$ mm^3 needed for SAW experiments, anisotropic fracture experiments were performed using high quality silicon crystals. The paper presents results obtained for the four crystallographic geometries Si(112)$<\bar{1}\,\bar{1}1>$, Si(111)$<\bar{1}\,\bar{1}2>$, Si(221)$<\bar{1}\,\bar{1}4>$, and Si(110)$<1\bar{1}1>$. The family of {111} planes provides the weakest cleavage planes in silicon. The selection of a particular crystal geometry and mode of loading defines the non-zero stress components acting on the corresponding chemical bonds. Thus the selection of a special crystallographic configuration is a crucial point of the experiment. Different geometries provide characteristic ratios of the various stress components in mixed-mode fracture, which can be determined by the SAW method.

Silicon (112): Initiation of impulsive fracture by nonlinear SAW pulses in the Si(112)$<\bar{1}\,\bar{1}1>$ geometry revealed that SAW pulses propagating in the $<\bar{1}\,\bar{1}1>$ direction induced fracture at significantly lower SAW amplitudes, and thus at lower laser pulse energy, than the mirror-symmetric wave propagating in the opposite $<11\bar{1}>$ direction [17]. This effect is a consequence of differences in the elastic nonlinearity of the two propagation directions. The easy-cracking configuration was used for fracture experiments with laser pulse energy of ~40 mJ. An optical microscope image of a typical fractured surface is presented in Fig. 2. The vertical line at the right-hand side is the imprint of the laser-generated line source. The position of the first probe spot was at a distance of ~0.5 mm from the source. With further propagation the finite SAW pulse developed the critical stress needed for failure. At a distance of ~1 mm from the source the first crack can be

seen. The crack field extending further to the left-hand side is the result of repetitive fracture processes, occurring due to repetitive recovery of the shock front after each fracture event.

On the surface the cracks extended into the $<1\bar{1}0>$ direction, perpendicular to the SAW propagation direction and sagittal plane, with a length of up to 50 µm. As expected, fracture occurred along the intersection line of the surface with the perpendicular $\{11\bar{1}\}$ cleavage plane (see Fig. 3). The measured signal, multiplied by the calibration factor, and the distance of 0.5 mm were used to solve the evolution equation and to predict the transient pulse profile at the first fracture location. This predicted profile was used for final stress calculations. The resulting peak value of the σ_{11} stress at the surface is associated with the tensile strength of the material. A series of experiments yielded ~4.5 GPa for the critical opening stress of silicon in this particular geometry. Note that here only normal stress acts on the $\{11\bar{1}\}$ cleavage plane, which is perpendicular to the surface, and consequently nucleation of failure can be considered as a pure mode I process.

Silicon (111): In the easy-cracking geometry Si(111) $<\bar{1}\bar{1}2>$ the fracture strength was in the range of ~4 GPa [15]. The surface−nucleated cracks propagated into the bulk along the $\{11\bar{1}\}$ cleavage plane, which is inclined by 19.5° to the normal of the free surface (see Fig. 3). According to the boundary conditions for SAWs, only the tensile opening stress σ_{11} is nonzero at the surface in the initial coordinate system, where x_1 points into the propagation direction and x_3 into the depth ('sagittal plane'). This tensile stress of $\sigma_{11} = 4$ GPa can be represented by a set of orthogonal components in the coordinate system associated with the tilted cleavage plane $\{11\bar{1}\}$. In fact, a combination of mode I (tensile opening) and mode II (in-plane shear sliding) processes is expected to control this fracture geometry. The resulting stress components for the biaxial fracture mechanism in the tilted coordinate system are $\sigma_{11}^T = 3.6$ GPa, $\sigma_{31}^T = -1.3$ GPa. In addition, a small contribution from the component $\sigma_{33}^T = 0.4$ GPa has to be taken into account in a rigorous treatment. Fig. 4 illustrates the biaxial fracture process along the $\{11\bar{1}\}$ cleavage plane.

Silicon (221): In this fracture geometry the tilt of the cleavage plane is 35.3° to the surface normal (see Fig. 4a)). A laser pulse energy of about 70 mJ had to be applied to achieve fracture in the easy cracking direction namely the Si(221)$<\bar{1}\bar{1}4>$ geometry. As the stress acting normal to the $\{11\bar{1}\}$ cleavage plane is reduced to 2/3 of the initial σ_{11} stress at the surface, all components can be easily obtained as described above as $\sigma_{11}^T = 0.67\ \sigma_{11}$, $\sigma_{31}^T = -0.48\ \sigma_{11}$, $\sigma_{33}^T = 0.33\ \sigma_{11}$. It is noteworthy that nearly half of the initial tensile stress is transformed to an in-plane-shearing action.

The optical microscope image of Fig. 6 presents the Si(221) plane after propagation of a cracking SAW pulse in the $<\bar{1}\bar{1}4>$ direction. The first crack is nucleated ~1 mm from the source. At a distance of ~3 mm from the sources several tracks generate a number of cracks extending to the left-hand side of the image. In contrast to the previous geometries, cracks consist of a line along $<1\bar{1}0>$ and two branches with an angle of ~70°. This angle is very close to the angle between the intersection lines of the $\{1\bar{1}1\}$ and $\{\bar{1}11\}$ cleavage planes with the surface, providing an example of crack bifurcation after nucleation. Numerical estimates show that these planes undergo failure induced by the following strong stress components: $\sigma_{11}^T = 0.67\,\sigma_{11}$, $\sigma_{22}^T = 0.31\,\sigma_{11}$, $\sigma_{21}^T = 0.45\,\sigma_{11}$, $\sigma_{31}^T = 0.13\,\sigma_{11}$, $\sigma_{32}^T = 0.09\,\sigma_{11}$, and $\sigma_{33}^T = 0.03\,\sigma_{11}$. The opening stress component σ_{11}^T has the same value as the opening stress component of the $\{11\bar{1}\}$ plane. These components bifurcate and draw cracks along the initial cleavage plane. Note that initial failure occurs along the line normal to the direction of the wave vector of the SAW pulse. This supports our basic assumption that tension of

chemical bonds normal to the cleavage plane is strongly involved in the process of crack nucleation while other stress components also influence the mechanical strength and may induce branching or draw tips along other cleavage planes. A critical tensile stress of σ_{11} of ~3.5 GPa was obtained for the Si(221)<$\overline{1}\,\overline{1}$4> geometry.

Silicon (110): It was demonstrated that transient SAW pulse evolution produces a steep shock front of $\partial u_3/\partial x_1$ in the Si(110)<1$\overline{1}$1> geometry (see Fig. 4b)). Calculations of the stress field resulted in a positive σ_{11} peak, which means that the acting forces stretch bonds normal to the cleavage plane. Moreover, there are displacements of particles along the x_2-coordinate axis, normal to the sagittal plane, which produce non-zero stress at the surface. The out-of-plane shearing component σ_{21} can be associated with fracture mode III and the σ_{22} stress stretches the material normal to the sagittal plane. These contributions, however, are relatively small, since the analysis yields $\sigma_{11}/\sigma_{21} \approx 15$ and $\sigma_{11}/\sigma_{22} \approx 7$ and for the peak stress components at the surface.

Dynamic fracture under the predominat action of biaxial stresses in the Si(110)<1$\overline{1}$1> geometry was studied to further examine mixed cases. There is no difference for nonlinear pulse evolution of counterpropagating SAWs in this particular geometry. Fracture could be achieved only by increasing the laser pulse energy up to ~150 mJ and no extensive crack field could be observed. The average value found for the initial critical tensile stress σ_{11} was ~7 GPa. The transformation of the coordinate system of the SAW solution to the fracture geometry gives the following estimates of the peak values of stress components for the second plane normal to the free surface, namely {$\overline{1}$11}, in comparison with the initial {1$\overline{1}$1} plane: $\sigma_{11}^T = 0.2\ \sigma_{11}$, $\sigma_{21}^T = 0.22\ \sigma_{11}$, and $\sigma_{22}^T = 0.95\ \sigma_{11}$. It turned out that these components are strong enough to branch the nucleated crack [16].

Discussion

The results clearly indicate that the choice of a defined geometry is crucial for a microscopic understanding of the complicated dynamic fracture behavior in anisotropic materials. The influence of boundary effects and the distinct surface confinement of guided SAWs provide unique conditions for controlled nonlinear pulse evolution and fracture that do not exist for elastic bulk waves and other methods. For the various geometries investigated in silicon, the observed tensile fracture strength varied between 3 and 7 GPa [15,16]. These values are in the same range as the critical fracture stresses observed in early loading experiments with a bearing ball on mirror−polished silicon wafers, yielding an average fracture stress of 2.8 GPa and a maximum value of 6.9 GPa [18]. Later on these results were confirmed with the same method, providing strengths between 2 and 8.8 GPa [19]. Such biaxial flexure tests, where the specimen is loaded centrally to generate an axisymmetric biaxial stress distribution, were recently employed to obtain strength data for silicon as a function of the fabrication process, yielding strengths in the range 1.2−4.6 GPa [20]. Thus we may conclude that the configurationally resolved and well defined fracture strengths are surprisingly similar to conventional configurationally averaged data. A reason for this finding is the fact that the system always selects the energetically lowest fracture configurations compatible with the initiating stress conditions.

The SAW results were obtained for the family of {111} cleavage planes of silicon. For these weakest planes an ideal tensile strength of 22 GPa and an ideal shear strength of 6.8 GPa of the {111} plane in the [112] direction has been found by *ab initio* calculations [1]. It is important to note that the quite low ideal shear stress is in the same range as the measured strength values. The SAW experiments revealed widespread multimode fracture mechanisms with a dominant tensile component during nucleation. Therefore, besides mode I, also mode II and mode III contributions

may play an important role. This suggests that the application of the one-dimensional Griffith model to determine flaw sizes, based on a pure tensile opening mechanism, must be considered with great care. In fact, an unrealistically large range of defect sizes has been reported for single-crystal silicon, extending from ~10 nm to ~10 μm [8,21]. The relatively small deviations between ideal and real strengths in silicon need a careful investigation of the fracture mechanism and simplified models based on uniaxial tension and the resulting fit parameters must be considered with great care.

For stress oriented in the [111] direction on the {111} cleavage plane, an ideal tensile strength of 95 GPa has been found and for shear on the {111} plane in the [112] direction an ideal shear strength of 93 GPa has been found for diamond by *ab initio* calculations [1]. It is important to note that the ideal tensile and shear strengths are essentially identical in cubic diamond. This distinct feature contributes to the outstanding mechanical properties of diamond. The situation in silicon, where the ideal shear stress is less than half of the ideal tensile stress, suggests an easy formation of dislocations [22]. In fact, dislocations have been observed at temperatures above 550°C in silicon [23,24].

The strength of diamond has mainly been studied by indentation methods because of small specimen sizes, but bursting disk tests and three-point bend tests have also been applied. Indentation experiments on good-quality natural diamonds yielded fracture strengths of approximately 4 GPa [9]. A similar value of 2.8 GPa has been reported previously [10]. Such a surprisingly low strength has also been confirmed by measurements on type IIa natural single-crystal diamond using a cantilever beam geometry, yielding 2.4 GPa [25]. In comparison with the strength of the ideal diamond lattice the real strength of available single-crystal diamond is one to two orders of magnitude smaller. Consequently, the nonlinear elastic behavior of diamond can be used as a very sensitive probe of the mechanical integrity of the lattice and may be employed for effective quality control. According to the 'weakest link' model, the material fails if the critical stress of the weakest link is reached. In this situation the strength is expected to increase with decreasing size of the volume or surface subjected to tensile and/or shear stresses.**Conclusions**

The contact-free and notch-free laser-based SAW technique introduced for studying dynamic fracture of brittle materials is an approach with several new features and applications. The absorption-layer technique and nanosecond laser pulses were used to launch nonlinear wideband SAW pulses with steep shock fronts. The induced dynamic fracture processes are characterized by a time scale in the nanosecond range, strains of ~0.01, and a non−uniform field of stresses with its maximum at the surface. In anisotropic materials the proper choice of the crystal geometry (crystallographic plane and direction) provides new insight into the anisotropy of the mechanical strength of solids. The experimental results presented for readily available high quality silicon crystals indicate a predominance of the tension stress component at the stage of surface nucleation of cracks. The strength values of 3−7 GPa obtained for the studied crystal geometries are in the range of the mean critical stresses determined for silicon wafers by bending and indentation methods and comparable to the ideal shear stress.

Owing to the quite low real fracture strength of diamond crystals of <9 GPa, the SAW method may also be applied to study the anisotropy of fracture in diamond if suitable crystal sizes and cuts are available. A comparison with silicon will provide important insight into the mechanical behavior of superhard materials with respect to the very different situation concerning the ratio between tensile and shear stress components in these two materials. This characteristic difference in the mechanical properties of silicon and diamond should become relevant in the ubiquitous multimode fracture processes, which controls the ultimate mechanical stability of materials.

Acknowledgments

References

[1]   D. Roundy and M. L. Cohen, Phys. Rev. B **64,** 212103 (2001).

[2]   Y. Umeno, A. Kushima, T. Kitamura, P. Gumbsch, and J. Li, Phys. Rev. B 72, 165431 (2005).

[3]   J. A. Hauch, D. Holland, M. P. Marder, and H. L. Swinney, Phys. Rev. Lett. 82, 3823 (1999).

[4]   T. Cramer, A. Wanner, and P. Gumbsch, Z. Metallkd. 90, 675 (1999).

[5]   R. Pérez and P. Gumbsch, Acta Mater. 48, 4517 (2000).

[6]   X. Li, T. Kasai, S. Nakao, T. Ando, M. Shikida, K. Sato, and H. Tanaka, Sens. Actuators A 117, 143 (2005).

[7]   R. Lawn, J. Mater. Res. 19, 22 (2004).

[8]   R. F. Cook, J. Mater. Sci. 41, 841 (2006)

[9]   J. E. Field and C. S. J. Pickles, Diamond Relat. Mater. 5, 625 (1996).

[10] J. E. Field, in The Properties of Diamond, J. E. Field (Ed.), Academic Press, London, 1979.

[11] A. R. Davies, J. E. Field, K. Takahashi, and K Hada, Diamond Relat. Mater. 14, 6 (2005).

[12] G. F. Cardinale and C. J. Robinson, J. Mater. Res. 7, 1432 (1992).

[13] R. Ikeda, H. Cho, M. Takemoto, and K. Ono, J. Acoust. Emission 22, 119 (2004).

[14] A. M. Lomonosov, A. P. Mayer, and P. Hess, in: Modern Acoustical Techniques for the Measurement of Mechanical Properties, M. Levy, H. E. Bass, and R. Stern (Eds.), Academic Press, San Diego, 2001, Vol. 1, pp. 65– 134.

[15] V. V. Kozhushko, A. M. Lomonosov, and P. Hess, Phys. Rev. Lett. 98, 195505 (2007).

[16] V. V. Kozhushko and P. Hess, Phys. Rev. B 76, 144105 (2007).

[17] A. M. Lomonosov and P. Hess, Phys. Rev. Lett. 89, 095501 (2002).

[18] S. M. Hu, J. Appl. Phys. 53, 3576 (1982).

[19] J. C. McClaughlin and A. F. W. Willoughby, J. Cryst. Growth 85, 83 (1987).

[20] K.-S. Shen, A. Ayon, and S. M. Spearing, J. Am. Ceram. Soc. 83, 1476 (2000).

[21] S. J. Glass, D. A. LaVan, T. E. Buchheit, and K. Jackson, Fractography of Glasses and Ceramics IV, J. R. Varner and G. D. Quinn (Eds.), The American Ceramic Society, Westerville, OH 2000, pp.227−240.

[22] D. Sherman and I. Be'ery, Phys. Rev. Lett. 93, 265501 (2004).

[23] J. Samuels and S. G. Roberts, Proc. R. Soc. Lond. A 421, 1 (1989).

[24] K. J. Hsia and A. S. Argon, Mater. Sci. Eng. A 176, 111 (1994).

[25]   C. S. J. Pickles, Diamond Relat. Mater. 11, 1913 (2002).
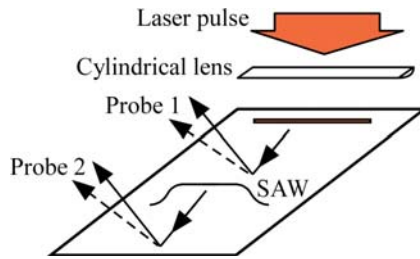
Figures

Fig. 1 Scheme of the pump–probe setup with pulsed laser excitation and cw laser probe-beam deflection at two spots.
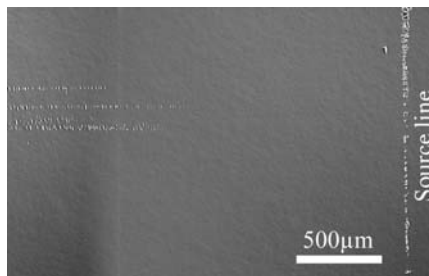

Fig. 2 Optical microscope image of the Si(112) plane with crack field, recorded after propagation of a single nonlinear SAW pulse with shock.
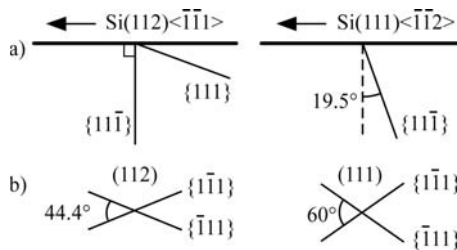

Fig. 3 Orientation of the {111} and {11$\bar{1}$} cleavage planes for the Si(112) and Si(111) cuts in sections along the (1$\bar{1}$0) sagittal plane (a) and top views of these cuts with the lines of intersection of the two cleavage planes {1$\bar{1}$1} and {$\bar{1}$11} with the free surface (b).
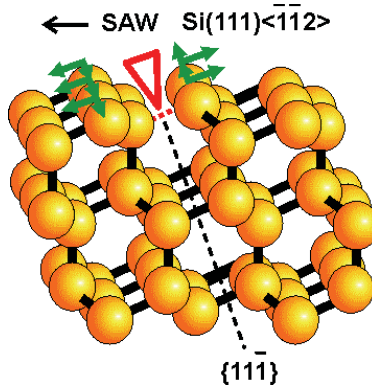
Fig. 4 Illustration of the crack nucleation process for the geometry Si(111)<$\bar{1}\bar{1}2$> with biaxial crack formation and propagation along the {11$\bar{1}$} cleavage plane, tilted by 19.5° to the surface normal.
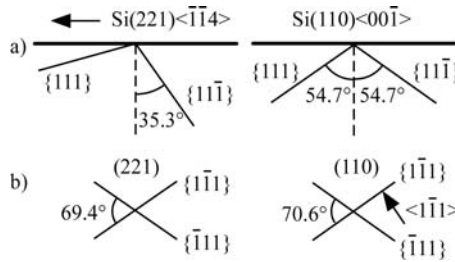

Fig. 5 Orientation of the {111} and {11$\bar{1}$} cleavage planes for the Si(221) and Si(110) cuts in sections along the (1$\bar{1}$0) sagittal plane (a) and top views of these cuts with the lines of intersection of the two cleavage planes {1$\bar{1}$1} and {$\bar{1}$11} with the free surface (b).
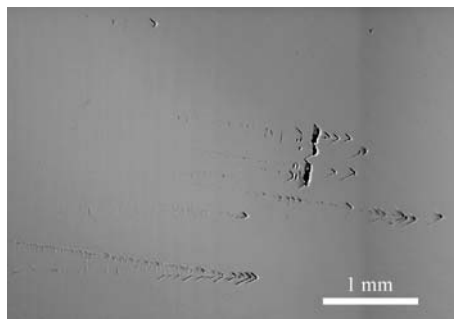

Fig. 6 Optical microscope picture of the Si(221) plane with the crack field after propagation of a single nonlinear SAW pulse.